Effect of normal contact forces on the stress in shear rate invariant particle suspensions

J. J. J. Gillissen* and H. J. Wilson
Department of Mathematics, University College London, Gower Street, London WC1E 6BT, United Kingdom

(Received 28 May 2018; published 2 January 2019)

We present a tensorial theory for the microstructure and the stress in shear rate invariant particle suspensions that includes hydrodynamic and normal but not tangential hard sphere interaction forces. The theory predicts that hydrodynamic forces produce a negligible first normal stress difference, while contact forces produce a positive first normal stress difference. The theory thereby provides a rationale for seemingly contradicting experimental observations in the literature. In addition, the theory captures the experimentally observed time dependence of the shear stress after shear reversal.

DOI: 10.1103/PhysRevFluids.4.013301

I. INTRODUCTION

Particle suspensions occur ubiquitously in nature, and their mechanical stress $\boldsymbol{\Sigma}$ is governed by the particle interaction forces, which can be classified into hydrodynamic and nonhydrodynamic. The nature of the hydrodynamic forces depends on the particle Reynolds number $\mathrm{Re}_p = \dot{\gamma} a^2/\nu$, where a is the particle radius, $\nu = \eta/\rho$ is the solvent kinematic viscosity, η is the solvent dynamic viscosity, ρ is the solvent mass density, and $\dot{\gamma}$ is the shear rate. When $\mathrm{Re}_p \ll 1$, flow inertia is negligible, and the hydrodynamic forces are governed by the linear Stokes equation.

The Stokes equation predicts that particles make no physical contacts in a fluid, since the lubrication force diverges at contact [1]. With increasing volume fraction ϕ, however, the lubrication films become progressively thinner, and when their thickness approaches the atomic length scale, the films may disintegrate, resulting in physical contacts.

This work addresses the effect of hard and frictionless contact forces on the particle stress. Hard contacts do not introduce a force scale F into the system, and the nondimensional suspension viscosity, $\Sigma_{12}/\eta\dot{\gamma}$, depends therefore only on the particle volume fraction ϕ and not on the shear rate $\dot{\gamma}$, as this cannot be nondimensionalized into $a^2\eta\dot{\gamma}/F$, due to the absence of F. This study is therefore restricted to shear rate invariant suspensions.

Experimental data on the suspension stress $\boldsymbol{\Sigma}$ are mainly concerned with shear flow, where $\boldsymbol{L} = \boldsymbol{\nabla U}^T = \dot{\gamma}\boldsymbol{\delta}_1\boldsymbol{\delta}_2$ is the velocity gradient tensor, $\dot{\gamma} = \sqrt{2\boldsymbol{E} : \boldsymbol{E}}$ is the shear rate, $\boldsymbol{E} = \frac{1}{2}(\boldsymbol{L} + \boldsymbol{L}^T)$ is the strain rate tensor, $\boldsymbol{U}$ is the velocity vector, and 1, 2, and 3 are the flow direction, the gradient direction, and the vorticity direction, respectively. Figure 1 summarizes experimental data on the relative first and second normal stress differences in shear rate invariant suspensions. These quantities are defined as $\zeta_1 = (\Sigma_{11} - \Sigma_{22})/\Sigma_{12}$ and $\zeta_2 = (\Sigma_{22} - \Sigma_{33})/\Sigma_{12}$, respectively. While ζ_2 has always been observed to be negative, ζ_1 has been observed to be both negative and small (compared to ζ_2) [5–7], as well as positive [2,4]. It is noted that a positive ζ_1 has also been observed in shear thickening suspensions [8–10], which supports the hypothesis that particle contact forces are responsible for $\zeta_1 > 0$ [11].

*jurriaangillissen@gmail.com

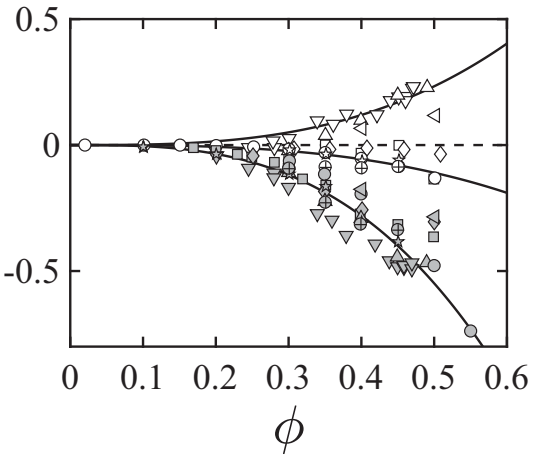

FIG. 1. Measured, steady, relative first and second normal stress differences $\zeta_1 = (\Sigma_{11} - \Sigma_{22})/\Sigma_{12}$ (open markers) and $\zeta_2 = (\Sigma_{22} - \Sigma_{33})/\Sigma_{12}$ (solid markers), under shear rate invariant conditions and as functions of the particle volume fraction ϕ. $\triangle$, $a = 20\,\mu$m; $\triangledown$, $a = 70\,\mu$m (polystyrene in water, UCON oil and zinc bromide [2]); $\square$, $a = 35\,\mu$m; $\diamond$, $a = 70\,\mu$m (polystyrene in poly(ethylene glycol-ran-propylene glycol) monobutylether [3]); $\triangleleft$, $a = 5\,\mu$m (poly (methyl methacrylate) (PMMA) in Triton X-100, anhydrous zinc chloride, and water (TZW) [4]); $\oplus$, $a = 98\,\mu$m (PMMA in TZW [5]); $\bigcirc$, $a = 22\,\mu$m (glass in corn syrup and glycerin [6]); and $\star$, $a = 20\,\mu$m (polystyrene in silicone fluid [7]). The lines are drawn to guide the eye, and the lower line represents the empirical relation [Eq. (16)].

In addition to normal stresses, effects of contact forces are also reflected by a stress discontinuity upon the reversal of shear flow. In the absence of contacts, the Stokes equation dictates that the stress is linear in the velocity. This means that when the flow velocity is instantaneously reversed, the stress is instantaneously reversed too, as observed experimentally for small ϕ [12]. For large ϕ, particles may experience contacts, and since contact forces are not reversed upon flow reversal, there is a discontinuity in the (absolute value of the) particle stress upon flow reversal [12–14].

In this work we provide a microstructural explanation for the above mentioned experimental observations, regarding normal stresses in steady shear flow, and stress discontinuity after shear reversal. To this end we include hard and frictionless contact forces into a previously proposed tensorial theory for the suspension microstructure and stress [15].

II. DERIVATION OF THE THEORY

A. Hydrodynamic forces

First we summarize the theory in the absence of contact forces. For a full derivation, the reader is referred to Ref. [15]. In the two-body approximation the stress is given by [16–19]

$$\boldsymbol{\Sigma} = -\frac{1}{V}\sum_{\alpha>\beta} \boldsymbol{F}_{\alpha,\beta}\boldsymbol{r}_{\alpha,\beta} = -n\langle \boldsymbol{F}\boldsymbol{r}\rangle. \tag{1}$$

Here $n = N/V$ is the particle number density, N is the number of particles inside the averaging volume V, $\boldsymbol{F}_{\alpha,\beta}$ is the interaction force $\boldsymbol{F}$ between particles α and β, and $\boldsymbol{r}_{\alpha,\beta}$ is the corresponding particle pair separation vector $\boldsymbol{r} = \boldsymbol{p}r$, where $\boldsymbol{p}$ is the particle pair orientation unit vector, and $r = |\boldsymbol{r}|$ is the particle pair separation. The stress is dominated by particle pairs with small gaps:

$$\boldsymbol{r} = 2a\,\boldsymbol{p}. \tag{2}$$

The interaction force $\boldsymbol{F}$,

$$\boldsymbol{F} = \boldsymbol{F}_h + \boldsymbol{F}_c, \tag{3}$$

is the sum of the hydrodynamic force $\boldsymbol{F}_h$ and the contact force $\boldsymbol{F}_c$, which is assumed zero, for the moment. The pair separation vector evolves as

$$\dot{\boldsymbol{r}} = c_1 \boldsymbol{L} : \boldsymbol{r}\boldsymbol{p}\boldsymbol{p} + \boldsymbol{L} \cdot \boldsymbol{r} \cdot (\boldsymbol{\delta} - \boldsymbol{p}\boldsymbol{p}), \tag{4}$$

and the corresponding lubrication force is to leading order

$$\boldsymbol{F}_h = -a^2 \eta c_2 \boldsymbol{E} : \boldsymbol{p}\boldsymbol{p}\boldsymbol{p}. \tag{5}$$

Here c_1 and c_2 are nondimensional functions of r/a and ϕ. Combining Eqs. (1), (2), (3), and (5) and using that $\phi \sim na^3$ gives the following particle stress tensor:

$$\boldsymbol{\Sigma} = \alpha \eta \boldsymbol{E} : \langle \boldsymbol{p}\boldsymbol{p}\boldsymbol{p}\boldsymbol{p} \rangle. \tag{6}$$

Here $\alpha = \tilde{c}_2 \phi$ is the lubrication stress parameter, and $\tilde{c}_2$ is the effective c_2, which is averaged over the distribution of pair configurations, and which diverges when ϕ approaches maximum packing.

The average $\langle \cdots \rangle$ in Eq. (6) is expressed as an integral over the probability distribution function $\Psi(\boldsymbol{r})$ of the particle pair separation vector $\boldsymbol{r}$:

$$\langle \cdots \rangle = \int_{|\boldsymbol{r}|=2a}^{|\boldsymbol{r}|=2a+\delta r} \Psi(\boldsymbol{r}) \cdots d^3\boldsymbol{r}, \tag{7}$$

where the integration is restricted to the so-called interaction shell, where particle pairs have small gaps: $0 < r - 2a < \delta r$. The evolution of $\Psi(\boldsymbol{r})$ is governed by the Smoluchowski equation:

$$\partial_t \Psi + \partial_k (\dot{r}_k \Psi) = 0. \tag{8}$$

Since computing $\Psi(\boldsymbol{r})$ is costly, we compute instead its second order orientation moment $\boldsymbol{a} = \langle \boldsymbol{p}\boldsymbol{p} \rangle$, referred to as the microstructure. The evolution equation for $\boldsymbol{a}$ is derived by inserting Eq. (4) into Eq. (8), multiplying the result by $\boldsymbol{p}\boldsymbol{p}$, and integrating the result from $r = 2a$ to $r = 2a + \delta r$ (see Ref. [15]):

$$\begin{aligned} \partial_t \langle \boldsymbol{p}\boldsymbol{p} \rangle = {} & \boldsymbol{L} \cdot \langle \boldsymbol{p}\boldsymbol{p} \rangle + \langle \boldsymbol{p}\boldsymbol{p} \rangle \cdot \boldsymbol{L}^T - 2\boldsymbol{L} : \langle \boldsymbol{p}\boldsymbol{p}\boldsymbol{p}\boldsymbol{p} \rangle \\ & - \beta \big[\boldsymbol{E}_e : \langle \boldsymbol{p}\boldsymbol{p}\boldsymbol{p}\boldsymbol{p} \rangle + \tfrac{1}{15} (2\boldsymbol{E}_c + \mathrm{Tr}(\boldsymbol{E}_c)\boldsymbol{\delta}) \big]. \end{aligned} \tag{9}$$

The first line of Eq. (9) described rotation of rigid dumbbells, i.e., fixed pair separations. The second line accounts for changes in the separation, which correspond to an orientation flux between the interaction shell and the exterior of this shell. This term is interpreted as the association and dissociation of interacting particle pairs, by the action of the compressive and the extensional parts of the rate of strain tensor, $\boldsymbol{E}_c$ and $\boldsymbol{E}_e$, respectively, which pushes particles together and pulls them apart, respectively. These effects are controlled by the pair association rate β, which is an increasing function of ϕ.

To close the theory a relation is needed to express the fourth order moment $\langle \boldsymbol{p}\boldsymbol{p}\boldsymbol{p}\boldsymbol{p} \rangle$ in terms of the second order moment $\langle \boldsymbol{p}\boldsymbol{p} \rangle$. Here we use the linear closure that was proposed in Ref. [20], which is accurate when the distribution is close to isotropy, such that $\Psi(\boldsymbol{p})$ is well captured by a linear expansion in the anisotropy tensor $\boldsymbol{a} - \boldsymbol{\delta}/3$, i.e., $\Psi(\boldsymbol{p}) = (4\pi)^{-1}[1 + \frac{15}{2}(\boldsymbol{a} - \boldsymbol{\delta}/3) : \boldsymbol{p}\boldsymbol{p}]$:

$$\begin{aligned} \langle p_i p_j p_k p_l \rangle = {} & -\tfrac{1}{35} \langle p_m p_m \rangle (\delta_{ij}\delta_{kl} + \delta_{ik}\delta_{jl} + \delta_{il}\delta_{jk}) \\ & + \tfrac{1}{7} (\delta_{ij} \langle p_k p_l \rangle + \delta_{ik} \langle p_j p_l \rangle + \delta_{il} \langle p_j p_k \rangle + \langle p_i p_j \rangle \delta_{kl} + \langle p_i p_k \rangle \delta_{jl} + \langle p_i p_l \rangle \delta_{jk}). \end{aligned} \tag{10}$$

B. Contact forces

Here, we extend the theory with hard and frictionless contact forces. We consider a limiting member of the class of shear rate invariant suspensions in which the interparticle friction coefficient

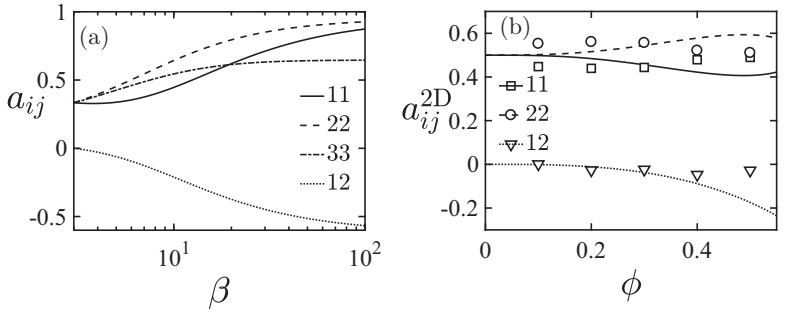

FIG. 2. (a) Modeled [Eqs. (9), (10)] microstructure $\boldsymbol{a}$ as a function of the pair association rate β. (b) Volume fraction ϕ dependence of the planar microstructure $\boldsymbol{a}^{2D}$, measured in Ref. [22] [Eq. (14), markers] and modeled [Eqs. (13), (15), and (16), lines].

vanishes and tangential friction forces may be ignored (see, e.g., Ref. [21]), and the microstructure equation [Eq. (9)] is unaffected by the contact forces. It is noted that, under shear thickening conditions, the tangential friction may have an effect on the particle motion, involving a transition from sliding to rolling friction, and these effects are not captured by the present theory.

By definition, the normal contact force $\boldsymbol{F}_c$ is directed along $\boldsymbol{p}$, i.e., $\boldsymbol{F}_c = |\boldsymbol{F}_c|\boldsymbol{p}$ when a particle pair is under compression, while it is zero, when a pair is under extension. The contact force magnitude $|\boldsymbol{F}_c|$ is therefore assumed to be proportional to the compressive part $\boldsymbol{E}_c$ of $\boldsymbol{E}$ projected onto $\boldsymbol{p}$, i.e., $|\boldsymbol{F}_c| = -c_3 a^2 \eta \boldsymbol{E}_c : \boldsymbol{pp}$, where c_3 is a nondimensional function of $\boldsymbol{p}$, and $a^2\eta$ is added to make the expression dimensionally correct:

$$\boldsymbol{F}_c = -c_3 a^2 \eta \boldsymbol{E}_c : \boldsymbol{ppp}. \tag{11}$$

Combining Eqs. (1)–(3), (5), and (11) and using that $\phi \sim na^3$ we arrive at the following particle stress tensor:

$$\boldsymbol{\Sigma} = \eta(\alpha \boldsymbol{E} + \chi \boldsymbol{E}_c) : \langle \boldsymbol{pppp} \rangle, \tag{12}$$

where $\chi = \tilde{c}_3 \phi$ is the contact stress parameter, and $\tilde{c}_3$ is the effective c_3, which is averaged over the distribution of pair configurations, and which diverges when ϕ approaches maximum packing.

III. THEORETICAL PREDICTIONS

A. Steady shear

In shear flow Eqs. (9) and (10) predict that particle pairs associate in the compressive quadrants $a_{12} < 0$, rotate towards x_2, and dissociate in the extensional quadrants $a_{12} > 0$. For $\beta > 3$, the association and dissociation dominate the rotation. The resulting distribution aligns in the compressive quadrant $a_{12} < 0$, with a slight tilt towards x_2, i.e., $a_{22} > a_{11}$. For $\beta < 3$, on the other hand, the pair rotation dominates the association and dissociation. Starting from isotropy, the resulting distribution oscillates and dampens towards a preferred alignment in the x_1 direction, corresponding to $a_{11} > a_{22}$ and $a_{12} > 0$. As these oscillations have not been observed in experiments, we restrict the following analysis to $\beta > 3$. The corresponding analytical solution to Eqs. (9) and (10),

$$\boldsymbol{a} = \left(6240 + 810\beta + 135\beta^2\right)^{-1} \times \begin{pmatrix} 3256 - 374\beta + 129\beta^2 & 252\beta - 84\beta^2 & 0 \\ 252\beta - 84\beta^2 & 904 + 410\beta + 129\beta^2 & 0 \\ 0 & 0 & 820 + 564\beta + 87\beta^2 \end{pmatrix}, \tag{13}$$

is plotted as a function of β in Fig. 2(a).

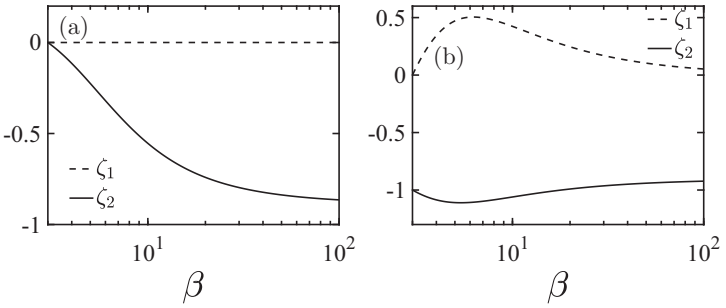

FIG. 3. Modeled [Eqs. (9), (10), and (12)] relative first normal stress difference $\zeta_1 = (\Sigma_{11} - \Sigma_{22})/\Sigma_{12}$ (dashed lines) and second normal stress difference $\zeta_2 = (\Sigma_{22} - \Sigma_{33})/\Sigma_{12}$ (solid lines), as functions of the pair association rate β for systems dominated by (a) hydrodynamic forces $(\alpha, \chi) = (1, 0)$ and (b) contact forces $(\alpha, \chi) = (0, 1)$.

In Fig. 2(b), we compare the modeled microstructure to experimental data from Ref. [22], reporting the planar, pair distribution function Ψ^{2D} in the (r_1, r_2) plane. In Fig. 2(b) the markers indicate the corresponding, measured, planar moments $\boldsymbol{a}^{2D}$:

$$\boldsymbol{a}^{2D} = \int_{|\boldsymbol{r}|=1.7a}^{|\boldsymbol{r}|=2.3a} \Psi^{2D}(\boldsymbol{r})\boldsymbol{p}\boldsymbol{p}d^2\boldsymbol{r}. \tag{14}$$

These measurement data show a weak departure from isotropy over the entire ϕ range, which supports the validity of the linear closure [Eq. (10)]. To compare our theory [Eq. (13)] to these experimental data, we convert the modeled volumetric moments $\boldsymbol{a}$ into the planar moments $\boldsymbol{a}^{2D}$ using

$$\boldsymbol{a}^{2D} = \frac{\boldsymbol{a}}{a_{11} + a_{22}}, \tag{15}$$

and we convert β to ϕ by using the modeled relation between β and ζ_2 [see Eq. (17) below, assuming $\chi = 0$], and the empirical relation

$$\zeta_2 = -4\phi^3, \tag{16}$$

which captures the experimental data shown in Fig. 1. In Fig. 2(b) the resulting modeled $\boldsymbol{a}^{2D}$ are plotted with the lines. Both experimental data and theory predict that $a_{12}^{2D} < 0$ and $a_{22}^{2D} > a_{11}^{2D}$.

The relative first and second normal stress differences are obtained by inserting Eq. (13) into Eqs. (10) and (12), giving

$$\begin{pmatrix}\zeta_1\\ \zeta_2\end{pmatrix} = \begin{pmatrix} \dfrac{336(\beta-3)\chi}{\alpha(54\beta^2-24\beta+904)+(63\beta^2-120\beta+452)\chi} \\ -\dfrac{48\alpha(\beta-3)\beta+(57\beta^2+6\beta+128)\chi}{\alpha(54\beta^2-24\beta+904)+(63\beta^2-120\beta+452)\chi} \end{pmatrix}, \tag{17}$$

which are plotted as functions of β for contactless systems, $(\alpha, \chi) = (1, 0)$, in Fig. 3(a), and for contact dominated systems, $(\alpha, \chi) = (0, 1)$, in Fig. 3(b). For systems without contact forces, we find $\zeta_1 = 0$ and $\zeta_2 < 0$ [Fig. 3(a)], and for systems with contact forces we find $\zeta_1 > 0$ and $\zeta_2 < 0$ [Fig. 3(b)]. These results may rationalize the data shown in Fig. 1 and suggest that the stress in Refs. [5–7] is dominated by hydrodynamic forces, while that in Refs. [2,4] is dominated by contact forces. It is further noted that the positive effect of contact forces on the first normal stress difference in shear invariant suspensions is supported by two dimensional Stokesian dynamics simulations in Ref. [23].

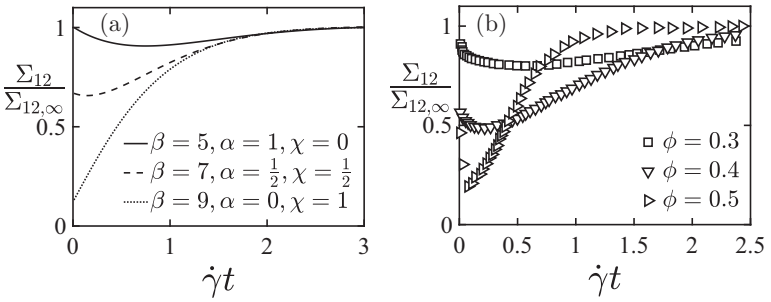

FIG. 4. (a) Modeled [Eqs. (9), (10), and (12)] suspension shear stress, scaled with the steady value $\Sigma_{12}/\Sigma_{12,\infty}$, as a function of the strain $\dot{\gamma}t$, after shear reversal, using various β, α, and χ. (b) Measured $\Sigma_{12}/\Sigma_{12,\infty}$ as a function of $\dot{\gamma}t$, after shear reversal, using various volume fractions ϕ [12].

The transition from negligible to significantly positive ζ_1 is explained as follows. The hydrodynamic part of the particle stress [Eq. (12)] produces a first normal stress difference,

$$\Sigma_{11} - \Sigma_{22} = \alpha\eta\dot{\gamma}(\langle p_1p_1p_1p_2\rangle - \langle p_2p_2p_2p_1\rangle), \tag{18a}$$

which is quadratic in the microstructure anisotropy and is therefore ignored by the linear closure [Eq. (10)], which predicts $\zeta_1 = 0$. The contact part of the particle stress, on the other hand, produces a first normal stress difference,

$$\Sigma_{11} - \Sigma_{22} = \chi\eta\dot{\gamma}\left[\tfrac{1}{2}\langle p_1p_1p_1p_2\rangle - \tfrac{1}{2}\langle p_2p_2p_2p_1\rangle + \tfrac{1}{4}\langle p_2p_2p_2p_2\rangle - \tfrac{1}{4}\langle p_1p_1p_1p_1\rangle\right], \tag{18b}$$

which is first order in the microstructure anisotropy, and according to the linear closure [Eq. (10)],

$$\Sigma_{11} - \Sigma_{22} = \tfrac{3}{14}\chi\eta\dot{\gamma}(a_{22} - a_{11}), \tag{18c}$$

which is positive, since $a_{22} > a_{11}$ [see Fig. 2(b)].

B. Shear reversal

Finally we consider the case of shear reversal. We use the Euler forward integration scheme with a time step of $\Delta t = 0.01/\dot{\gamma}$ to compute the time dependent microstructure and stress after shear reversal, using various values for β, α, and χ. In the computation, the initially isotropic suspension $\boldsymbol{a} = \boldsymbol{\delta}/3$ is sheared until a steady state is reached, after which the flow direction is reversed from negative to positive, at which instant we define $t = 0$. The reversal induces a reorganization of the microstructure and the attainment of a new steady state.

The modeled shear stress, scaled with the steady value $\Sigma_{12}/\Sigma_{12,\infty}$, is plotted as a function of the strain $\dot{\gamma}t$ in Fig. 4(a). As expected, the stress in the contactless theory, $(\alpha, \chi) = (1, 0)$, is conserved upon shear reversal, followed by a decrease and subsequent recovery to the steady value. In the contact dominated theory, $(\alpha, \chi) = (0, 1)$, on the other hand, the shear stress is not conserved upon shear reversal; i.e., there is a discontinuous drop, followed by a recovery, in qualitative agreement with experimental data from the literature [12], which are plotted in Fig. 4(b). The qualitatively correct prediction of the stress discontinuity, which is related to the contact forces, further validates the physical significance of the proposed constitutive equations [Eqs. (9), (10), and (12)].

IV. CONCLUSION

We propose a tensorial theory for suspension microstructure and stress that includes both hydrodynamic and hard sphere interaction forces.

The theory assumes hard and frictionless contact forces, which is a reasonable assumption for shear rate invariant suspensions but may not be valid for shear thickening suspensions. The theory

furthermore assumes a linear relationship between the stress and the microstructure anisotropy [Eq. (10)], which is supported by experimental data in the literature [22], as illustrated in Fig. 2(b).

The theory predicts that hydrodynamic forces produce a negligible first normal stress difference ζ_1, while contact forces produce a positive ζ_1. These results may provide a rationale for seemingly contradicting experimental observations in the literature, as illustrated in Fig. 1.

ACKNOWLEDGMENT

We would like to acknowledge financial support from the Engineering and Physical Sciences Research Council of the United Kingdom Grant No. EP/N024915/1.

[1] S. Kim and S. Karilla, *Microhydrodynamics* (Butterworth-Heinemann, Boston, 1991).
[2] T. Dbouk, L. Lobry, and E. Lemaire, Normal stresses in concentrated non-Brownian suspensions, J. Fluid Mech. **715**, 239 (2013).
[3] É. Couturier, F. Boyer, O. Pouliquen, and É. Guazzelli, Suspensions in a tilted trough: Second normal stress difference, J. Fluid Mech. **686**, 26 (2011).
[4] C. Gamonpilas, J. F. Morris, and M. M. Denn, Shear and normal stress measurements in non-Brownian monodisperse and bidisperse suspensions, J. Rheol. **60**, 289 (2016).
[5] A. Singh and P. R. Nott, Experimental measurements of the normal stresses in sheared Stokesian suspensions, J. Fluid Mech. **490**, 293 (2003).
[6] I. E. Zarraga, D. A. Hill, and D. T. Leighton, Jr., The characterization of the total stress of concentrated suspensions of noncolloidal spheres in Newtonian fluids, J. Rheol. **44**, 185 (2000).
[7] S.-C. Dai, E. Bertevas, F. Qi, and R. I. Tanner, Viscometric functions for noncolloidal sphere suspensions with Newtonian matrices, J. Rheol. **57**, 493 (2013).
[8] D. Lootens, H. Van Damme, Y. Hémar, and P. Hébraud, Dilatant Flow of Concentrated Suspensions of Rough Particles, Phys. Rev. Lett. **95**, 268302 (2005).
[9] J. R. Royer, D. L. Blair, and S. D. Hudson, Rheological Signature of Frictional Interactions in Shear Thickening Suspensions, Phys. Rev. Lett. **116**, 188301 (2016).
[10] L. C. Hsiao, S. Jamali, E. Glynos, P. F. Green, R. G. Larson, and M. J. Solomon, Rheological State Diagrams for Rough Colloids in Shear Flow, Phys. Rev. Lett. **119**, 158001 (2017).
[11] M. Wyart and M. E. Cates, Discontinuous Shear Thickening Without Inertia in Dense Non-Brownian Suspensions, Phys. Rev. Lett. **112**, 098302 (2014).
[12] F. Blanc, F. Peters, and E. Lemaire, Local transient rheological behavior of concentrated suspensions, J. Rheol. **55**, 835 (2011).
[13] C. Ness and J. Sun, Two-scale evolution during shear reversal in dense suspensions, Phys. Rev. E **93**, 012604 (2016).
[14] F. Peters, G. Ghigliotti, S. Gallier, F. Blanc, E. Lemaire, and L. Lobry, Rheology of non-Brownian suspensions of rough frictional particles under shear reversal: A numerical study, J. Rheol. **60**, 715 (2016).
[15] J. J. J. Gillissen and H. J. Wilson, Modeling sphere suspension microstructure and stress, Phys. Rev. E **98**, 033119 (2018).
[16] J. D. Goddard, An elastohydrodynamic theory for the rheology of concentrated suspensions of deformable particles, J. Non-Newtonian Fluid Mech. **2**, 169 (1977).
[17] B. H. A. A. Van den Brule and R. J. J. Jongschaap, Modeling of concentrated suspensions, J. Stat. Phys. **62**, 1225 (1991).
[18] N. Phan-Thien, Constitutive equation for concentrated suspensions in Newtonian liquids, J. Rheol. **39**, 679 (1995).
[19] R. C. Ball and J. R. Melrose, A simulation technique for many spheres in quasi-static motion under frame-invariant pair drag and Brownian forces, Phys. A (Amsterdam, Neth.) **247**, 444 (1997).

[20] E. J. Hinch and L. G. Leal, Constitutive equations in suspension mechanics. Part 2. Approximate forms for a suspension of rigid particles affected by Brownian rotations, J. Fluid Mech. **76**, 187 (1976).
[21] R. Seto and G. G. Giusteri, Normal stress differences in dense suspensions, J. Fluid Mech. **857**, 200 (2018).
[22] F. Blanc, E. Lemaire, A. Meunier, and F. Peters, Microstructure in sheared non-Brownian concentrated suspensions, J. Rheol. **57**, 273 (2013).
[23] H. Wilson and R. Davis, Shear stress of a monolayer of rough spheres—corrigendum, J. Fluid Mech. **814**, 614 (2017).